

GRPO Privacy Is at Risk: A Membership Inference Attack Against Reinforcement Learning With Verifiable Rewards

Yule Liu¹ Heyi Zhang² Jingyi Zheng¹ Zhen Sun¹ Zifan Peng¹
Tianshuo Cong³ Yilong Yang^{4†} Xinlei He^{1†} Zhuo Ma⁴

¹The Hong Kong University of Science and Technology (Guangzhou)

²Shanghai Jiao Tong University ³Shandong University ⁴Xidian University

Abstract

Membership inference attacks (MIAs) on large language models (LLMs) pose significant privacy risks across various stages of model training. Recent advances in Reinforcement Learning with Verifiable Rewards (RLVR) have brought a profound paradigm shift in LLM training, particularly for complex reasoning tasks. However, the on-policy nature of RLVR introduces a unique privacy leakage pattern: since training relies on self-generated responses without fixed ground-truth outputs, membership inference must now determine whether a given prompt (independent of any specific response) is used during fine-tuning. This creates a threat where leakage arises not from answer memorization.

To audit this novel privacy risk, we propose **Divergence-in-Behavior Attack (DIBA)**, the first membership inference attack specifically designed for RLVR. DIBA shifts the focus from memorization to behavioral change, leveraging measurable shifts in model behavior across two axes: advantage-side improvement (e.g., correctness gain) and logit-side divergence (e.g., policy drift). Through comprehensive evaluations, we demonstrate that DIBA significantly outperforms existing baselines, achieving around 0.8 AUC and an order-of-magnitude higher TPR@0.1%FPR. We validate DIBA’s superiority across multiple settings—including indistribution, cross-dataset, cross-algorithm, black-box scenarios, and extensions to vision-language models. Furthermore, our attack remains robust under moderate defensive measures.

To the best of our knowledge, this is the first work to systematically analyze privacy vulnerabilities in RLVR, revealing that even in the absence of explicit supervision, training data exposure can be inferred through behavioral traces.

1 Introduction

Large language models (LLMs) have demonstrated remarkable capabilities across diverse tasks [1, 2], including academic writing [3], code generation [4], and question answering [5]. Modern LLMs are typically trained through a three-

Stage	Training Objective	Inference Target	MIA Signal
Pre-training [12,13,17,18]	Language Modeling	Text Segment	Memorization-based Attack → Loss / Fluency Gap
SFT [15,16]	Conditional Generation (query → answer)	Query-Answer Pair	
Preference-based RL [14]	Maximize Human Preference	Query-Preferred-Rejected Triple	Preference-gap Attack → $\log P(\text{chosen}) - \log P(\text{rejected})$
RL RLVR (Ours)	Maximize Rule-based Reward	Prompt (Query) (no response given)	Divergence-in-Behavior Attack → Advantage Signal + Divergence Signal

Figure 1: MIAs in different LLM training paradigms.

stage paradigm [6, 7]: pre-training, supervised fine-tuning (SFT), and reinforcement learning (RL). Specifically, Reinforcement Learning with Verifiable Rewards (RLVR) [1, 8–10], a recently developed new family of RL algorithms, has brought a significantly profound paradigm shift in the game of LLMs. Almost all mainstream LLMs [1, 2, 11] are employing RLVR as their last step in the pipeline.

During the training procedure, models ingest trillions of tokens, which are often drawn from public but privacy-sensitive sources, to enable broad linguistic understanding [5, 12]. Given this extensive data exposure, ensuring that trained models do not inadvertently leak information about their training data has become a critical concern. Recent work has shown that each stage of the training pipeline introduces distinct privacy risks, prompting the development of numerous membership inference attack (MIA) techniques to audit data exposure [13–17]. Due to fundamental differences in training objectives and data structures, the adversary’s goal varies significantly across stages. We compare the difference across MIA in different training paradigms in Figure 1, with each having a different inference target (detailed in Section 2).

However, RLVR’s new training diagram [1, 9] introduces unique privacy risks. RLVR does not rely on human-provided preferences or exact reference answers. Instead, it generates multiple responses to a given prompt and uses simple, automated rules (e.g., checking whether a math answer is correct) to assign a binary reward (0 or 1) to each response. The model is then updated to favor responses that receive a reward of 1. This approach requires only a verifiable final answer—not a step-by-step “ground truth”—and avoids explicit token-by-token memorization. *As a result, traditional attacks that exploit memorization of the ground-truth*

[†]Corresponding authors: Yilong Yang (yangyilong@xidian.edu.cn) and Xinlei He (xinleihe@hkust-gz.edu.cn).

response become ineffective (typically achieving $AUC < 0.6$, see Table 1). In this challenging RLVR scenario, privacy leakage no longer manifests through memorization of specific outputs. Instead, it emerges as subtle behavioral changes, i.e., slight differences in how the model handles certain inputs. This behavioral divergence between the base and fine-tuned models constitutes a new threat surface and provides a more generalizable dimension for membership inference attacks. To the best of our knowledge, we are the first work to study membership inference in this challenging and realistic RLVR scenario.

To address the unique privacy challenges posed by RLVR, we propose **Divergence-in-Behavior Attack (DIBA)**, a novel membership inference framework that shifts focus from memorization to behavioral change. Instead of relying on memorization features, such as likelihood or output fluency, DIBA quantifies the divergence in behavioral changes along two complementary axes:

- The advantage side, which captures improvements in correctness (i.e., reward gain), contributing strongly to overall discriminative power (AUC);
- The logit side, which measures changes in token-level probabilities, providing calibrated, high-precision signals crucial for low-FPR detection.

Compared to existing baselines, DIBA achieves an order-of-magnitude improvement in $TPR@0.1\%FPR$ while maintaining strong AUC (up to 0.84), demonstrating its superior effectiveness in high-precision, privacy-sensitive settings. The attack generalizes well across datasets, transferring robustly from harder (e.g., paraphrased) to easier ones, indicating resilience to surface-form variations. Additionally, we find that transferring across different algorithms has a larger influence on attack performance than model sizes. When extended to vision-language models (VLMs), DIBA remains effective with an AUC of approximately 0.7, confirming the presence of behavioral signals in multimodal settings, while $TPR@0.1\%FPR$ is notably lower. Ablation studies reveal that sufficient response sampling and moderate temperature are crucial for reliable feature estimation. Moreover, using responses sampled from the fine-tuned model yields stronger logit-side signals than those from the base model, further emphasizing the importance of targeting learned behaviors.

We find that membership leakage is strongest on prompts that exhibit measurable behavioral change during training, and weakest on consistently correct or incorrect prompts. This underscores that behavioral divergence, not static correctness, is the primary driver of inference success. Our analysis shows that prompts with pre-existing high correctness can lead to elevated false positives, reflecting how RLVR amplifies inherent model capabilities. Additionally, we evaluate three practical defenses. DIBA exhibits decent robustness against these potential defenses, and only the paraphrase attack can effectively reduce the performance, which is at a steep computation cost.

In summary, we make the following contributions:

- We are the first to reveal the privacy risk in RLVR, tackling a challenging threat model where only prompts, not

responses, are targeted.

- We propose DIBA, a new paradigm for MIA that captures the behavioral divergence instead of the memorization after training, to audit the privacy leakage within RLVR.
- We conduct an extensive evaluation of DIBA across in-distribution, cross-dataset, cross-algorithm, and extension to VLMs settings, and demonstrate both the effectiveness of behavioral divergence as a leakage signal.

2 Related Work

Reinforcement Learning for LLM. Extensive studies have shown the superior ability of LLM across various domains and tasks, such as academic writing [3, 5], code generation [4, 11], and math reasoning [1], which mainly stem from the well-known three-stage training process [6], i.e., pre-training, supervised fine-tuning (SFT), and reinforcement learning (RL). Specifically, SFT is believed to memorize the training data and struggles to generalize out-of-distribution, while RL, in contrast, can generalize to unseen variants of queries [18]. Current RL algorithms can be mainly divided into two parts: preference-based RL and Reinforcement Learning with Verifiable Rewards (RLVR).

Regarding preference-based RL, it is featured by explicitly or implicitly deriving the reward from pairwise data. Two representative methods are PPO [19] and DPO [20]. Proximal Policy Optimization (PPO) [21] is a popular actor-critic algorithm used to fine-tune language models with feedback from a reward model. It first trains a reward model on a large scale of pairwise preference data, followed by utilizing the reward signal to optimize the LLM (the actor) while a value function (the critic) helps to stabilize the training process. To simplify the complexity and save the training cost of PPO, Direct Preference Optimization (DPO) [20] was introduced as a more direct method. DPO refactors the alignment problem to eliminate the need for an explicit reward model. Instead, it directly optimizes the LLM using a simple classification loss on pairs of preferred and dispreferred responses, effectively treating the LLM itself as a reward model.

Regarding RLVR, it is featured by computing the reward by a rule-based verification function and no longer needs the preference data. It enables the LLMs to have the capability of test-time scaling, thus having longer reasoning paths and stronger reasoning ability [1, 9, 22]. Specifically, it first samples a group of outputs for a given prompt and computes the advantage of each response for updating the policy. Since the advantages are computed using rule-based reward, e.g., exact match of math answer or execution results of code, RLVR can significantly reduce the required resources. We will introduce the RL algorithms on LLMs in Section 3.

Membership Inference on Pre-training Data. We denote the LLM as a policy (π_θ) that generates different actions (responses o) given certain states (prompt q). The base model is referred to as π_{ref} . In the pre-training stage, adversaries seek to determine whether a given text or paragraph (e.g., a Wikipedia passage) was present in the pre-training corpus [13, 14, 23–25]. Studies in this setting are typically conducted on early LLMs with identifiable data sources, such

as GPT-2 [26] and Pythia [27]. The dataset is partitioned into member and non-member samples based on the model’s knowledge cutoff time. Several representative methods are shown in MIAs at this stage primarily exploit the model’s increased fluency or lower perplexity on data it has seen during pre-training.

Membership Inference on SFT Data. In the SFT stage, the goal is to infer whether a specific question-answer pair (q, o) , comprising query q and the response o , is included in the SFT dataset. Attacks here mainly leverage the model’s tendency to memorize and overfit to seen training samples, leading to distinguishable behavioral patterns on member inputs [16, 17, 28]. The methods on pre-training data can be seamlessly transferred by replacing the probability term $\pi_\theta(q)$ with the conditional probability $\pi_\theta(o|q)$. Additionally, we list several methods optimized for SFT data.

- **SPV-MIA [16]:** It first computes the neighborhood score by $\text{Score}_{\text{Nei}}(q, \pi_\theta) = \frac{1}{N} \sum \log \pi_\theta(\hat{q}) - \log \pi_\theta(q)$, where the \hat{q} is the collection of multiple paraphrased version of prompt q . Then, it trains a self-prompted model π_{sp} to calibrate the neighborhood score function, i.e.,

$$\text{Score}_{\text{SPV-MIA}} = \text{Score}_{\text{Nei}}(q, \pi_{sp}) - \text{Score}_{\text{Nei}}(q, \pi_\theta)$$

- **LoRA-Leak [17]:** It enhances the MIA score by calibrating with the base model just as LiRA does. Compared to using the score derived only from the fine-tuned model, calibrating the score with the base model can make the membership signal more distinguishable.

Membership Inference on Preference Data. Regarding the preference-based RL, the goal is to train a reward model and update the policy to assign a higher probability to preferred responses. Adversaries aim to determine whether particular “query-preferred-rejected” data $(q, o_{\text{prefer}}, o_{\text{reject}})$, comprising query q , a preferred response o_{prefer} , and a rejected response o_{reject} , is used during reward modeling or policy optimization. The corresponding MIA targets triplets and leverages the gap in likelihoods between chosen and unchosen responses to infer membership. A representative approach is PREMIA [15], which quantifies the model’s advantage for the preferred response over the rejected one.

$$\text{Score}_{\text{PREMIA}} = \frac{\pi_\theta(o_{\text{prefer}}|q)}{\pi_{\text{ref}}(o_{\text{prefer}}|q)} - \frac{\pi_\theta(o_{\text{reject}}|q)}{\pi_{\text{ref}}(o_{\text{reject}}|q)}$$

MIAs in this context exploit the model’s stronger preference for the chosen response over the rejected one, often reflected in probability gaps or response rankings.

3 Preliminary for RL

In this section, we will introduce the notation and formulation of different RLVR algorithms that are widely used in training foundation models, including GRPO, and DAPO.

GRPO [1]. It is a recent RL algorithm designed to retain the benefits of online reinforcement learning while significantly reducing the resource burden of PPO. Instead of learning a value function for baseline estimation, GRPO uses a

group-based baseline. Specifically, for each prompt q , it samples multiple responses $\{o_1, \dots, o_G\}$ from the current policy, scores them with a rule-based function (e.g., check if the response correctly answers the math problem), and normalizes the rewards by subtracting the group mean and dividing by the group standard deviation. Formally, the advantage of each token in the response is computed by: $\hat{A}_{i,t} = \frac{r_i - \text{mean}(\mathbf{r})}{\text{std}(\mathbf{r})}$, where r_i is the indicator function to show if the response contains the correct answer. The GRPO objective is:

$$\mathcal{J}(\theta) = \mathbb{E}_{[q, \{o_i\}_{i=1}^G \sim \pi_{\theta_{\text{old}}}] } \frac{1}{G} \sum_{i=1}^G \frac{1}{|o_i|} \sum_{t=1}^{|o_i|} \left(\frac{\pi_\theta(o_{i,t} | q, o_{i,<t})}{\pi_{\theta_{\text{old}}}(o_{i,t} | q, o_{i,<t})} \hat{A}_{i,t} - \beta D_{\text{KL}}(\pi_{\text{ref}}, \pi_\theta) \right), \quad (1)$$

where D_{KL} is the KL divergence, and π_{ref} is the reference model (e.g., the initial model), β controls the strength of regularization.

DAPO [9]. A widely adopted variant of GRPO is DAPO, which improves training stability through several key modifications. It introduces clip-higher, which decouples the upper and lower clipping bounds to stabilize policy updates. The rebalancing act mechanism gives longer sequences greater influence in the gradient computation. Dynamic sampling filters out prompts with perfect or zero accuracy within each batch, ensuring non-zero advantages and meaningful learning signals. Additionally, overlong reward shaping penalizes excessively long responses to improve efficiency. Notably, DAPO sets the KL divergence regularization term to zero, distinguishing it from other RLVR methods that rely on divergence-based constraints.

$$\mathcal{J}(\theta) = \mathbb{E}_{[q, \{o_i\}_{i=1}^G \sim \pi_{\theta_{\text{old}}}] } \left[\underbrace{\frac{1}{\sum_{i=1}^G |o_i|} \sum_{i=1}^G \sum_{t=1}^{|o_i|} \frac{\pi_\theta(o_{i,t} | q, o_{i,<t})}{\pi_{\theta_{\text{old}}}(o_{i,t} | q, o_{i,<t})} \hat{A}_{i,t}^{\text{clipped}}}_{\text{Rebalancing Act}} \right] + \underbrace{R_l(\{o_i\}_{i=1}^G)}_{\text{Overlong Punish}}, \quad (2)$$

s.t. $\underbrace{0 < |\{o_i | \text{is_correct}(o_i)\}|}_{\text{Dynamic Sampling}} < G$

Comparison Across RL Algorithms. RLVR algorithms differ fundamentally from both preference-based RL and SFT in two key aspects. First, as on-policy methods, they generate responses (i.e., actions) by directly sampling from the LLM (policy), rather than relying on a fixed dataset of expert or “golden” answers. This eliminates the need for answer templates and renders traditional memorization-based membership inference attacks ineffective, as there is no static target for the model to memorize. Second, unlike PPO and DPO, which depend on the pairwise preference data, RLVR employs a rule-based reward function derived from non-pairwise verifiable outcomes (e.g., correctness checks). Consequently, attacks that rely on inferring membership from preference data are not applicable.

Table 1: Baseline performance adapted from memorization-based MIA.

Method	GRPO-3B		DAPO-3B		GRPO-7B		DAPO-7B	
	AUC	TPR@0.1%FPR	AUC	TPR@0.1%FPR	AUC	TPR@0.1%FPR	AUC	TPR@0.1%FPR
LOSS	0.572	0.002	0.570	0.002	0.582	0.005	0.589	0.002
LiRA	0.506	0.008	0.503	0.005	0.565	0.013	0.581	0.006
Zlib	0.558	0.000	0.555	0.000	0.563	0.000	0.565	0.002
↔ + Calibrate	0.509	0.000	0.508	0.000	0.550	0.009	0.563	0.005
Min-K%	0.511	0.000	0.533	0.000	0.512	0.003	0.520	0.002
↔ + Calibrate	0.539	0.003	0.543	0.002	0.501	0.003	0.510	0.002
Entropy	0.591	0.002	0.591	0.002	0.586	0.000	0.583	0.002
↔ + Calibrate	0.529	0.006	0.506	0.005	0.593	0.008	0.566	0.009
Neighbor	0.518	0.006	0.518	0.003	0.514	0.002	0.507	0.002
Ours	0.713	0.073	0.835	0.154	0.749	0.084	0.819	0.107

4 MIA Against RLVR

In this section, we first discuss the threat model. Then we revisit the membership inference target and demonstrate how existing memorization-based attack strategies fail in the RLVR setting.

4.1 Threat Model

Regarding the threat model, we adopt the setting established in prior work [16, 17, 28, 29], where the victim utilizes the private dataset to fine-tune a publicly available pre-trained model, such as those from the Qwen or Llama families, and subsequently releases the fine-tuned model weights (π_θ) to public model repositories like HuggingFace.

Adversary’s Goal. The adversary’s goal is to determine whether a given query (prompt) q , not responses, is part of the training dataset used during the RLVR fine-tuning phase. Specifically, the membership inference is targeted solely at the RLVR training data, only comprising the prompts (query) used in the on-policy sampling process, and does not include the step-by-step ground truth. This reflects a realistic threat model where the adversary seeks to expose the proprietary prompts used in RLVR.

Adversary’s Knowledge and Capability. We adopt the most widely used setting in MIA for LLMs [13–16, 24]. Specifically, we consider a grey-box attack scenario in which the adversary has access to the token-wise logits of the target LLM, enabling the computation of various inference metrics. However, the adversary does not have white-box access. They cannot observe or compute gradients during fine-tuning, nor do they have control over the training process. Regarding the fine-tuning procedure, the adversary knows only that the model was trained using an RLVR algorithm, but has no knowledge of the specific variant or training hyperparameters (e.g., learning rate, batch size, or sampling strategy). Crucially, according to the licensing terms of mainstream LLMs [30, 31], users are required to disclose the base model when releasing a fine-tuned version. As a result, the adversary can reliably determine the exact pre-trained model used as the foundation. Specifically, the adversary can know if the final answer is correct or is rewarded. Since the verifiers are typically public [32–34], knowledge of verifi-

cation signals (correct/incorrect) does not leak the original dataset’s hidden annotation structure.

4.2 Failure of Memorization-based Attacks

We will first show the ineffectiveness of existing membership inference attacks under the RLVR setting from a gradient perspective.

Analysis From Gradients Perspective. The analytical gradient of SFT is shown as:

$$\nabla_{\theta} \mathcal{J}(\theta) = \mathbb{E}_{[q, o \sim \mathcal{D}]} \sum_{t=1}^{|o|} \nabla_{\theta} \log \pi_{\theta}(o_t | q, o_{<t}), \quad (3)$$

where \mathcal{D} is the fine-tuning dataset. Each gradient update is directed toward maximizing the log-likelihood of a ground-truth response o associated with input q . Because the optimization process repeatedly reinforces this specific output sequence, the fine-tuned model exhibits strong and measurable membership signals for inputs that appear in \mathcal{D} . However, RLVR presents a fundamentally different privacy landscape. The analytical gradient of GRPO algorithm is shown as:

$$\nabla_{\theta} \mathcal{J}(\theta) = \mathbb{E}_{[q, \{o_i\}^G \sim \pi_{\theta, old}]} \frac{1}{G} \sum_{i=1}^G \frac{1}{|o_i|} \sum_{t=1}^{|o_i|} m_{i,t} \nabla_{\theta} \log \pi_{\theta}(o_{i,t} | q, o_{i,<t}) \quad (4)$$

where the gradient coefficient $m_{i,t}$ is defined as follows:

$$m_{i,t} = \underbrace{\hat{A}_{i,t}}_{\text{Advantage Term}} + \beta \underbrace{\left(\frac{\pi_{ref}(o_{i,t} | o_{i,<t})}{\pi_{\theta}(o_{i,t} | o_{i,<t})} - 1 \right)}_{\text{Divergence Term}} \quad (5)$$

Given the analytical gradient formula, responses are generated on-policy by sampling from the LLM itself, without reliance on fixed reference answers. As a result, the only consistent and static component of the training data is the input prompt q . This training paradigm renders conventional membership signals (e.g., answer memorization or preference alignment) ineffective.

Empirical Evaluation. Given the inherent challenge of our threat model, where only prompts (without reference answers) are available to the adversary, we intentionally relax

the attacker’s capabilities to create a favorable evaluation scenario: we assume access to ground-truth reference answers for each prompt. This transforms the task into one resembling SFT, where likelihood-based methods should perform well if memorization were a dominant signal. Detailed experimental details are provided in Section 6, and hyperparameter settings for baseline implementations are reported in Section C.

Despite this advantage, all baseline methods, as well as their calibrated variants (calibrating with the same metric computed by the base model), achieve poor performance close to random guessing. As shown in Table 1, the best-performing baseline does not exceed an AUC of 0.6, even with full answer knowledge. This near-total failure of traditional MIA techniques underscores a key insight: in RLVR, membership signals do not arise from memorization of specific outputs, and thus cannot be captured simply by likelihood-based metrics. The results confirm that the memorization-based paradigm fails to audit the privacy leakage under the current threat model.

5 Divergence-in-Behavior Attack (DIBA)

Unlike membership inference in pre-training or SFT, where overfitting and memorization provide strong signals for identifying training data, such cues are largely absent in RLVR. In this setting, responses are generated on-policy and evaluated via rule-based rewards rather than fixed ground-truth answers, significantly reducing the model’s reliance on explicit memorization. As a result, we can no longer exploit typical indicators such as likelihood overfitting or answer repetition to infer membership.

Instead, we *characterize the more subtle ways in which the fine-tuned model’s behavior diverges from that of the base model—shifts that arise not from rote memorization, but from policy optimization guided by verifiable outcomes*. This makes membership inference in RLVR a far more complex and challenging task. To address this challenge, we revisit the training dynamics of RLVR algorithms.

Preparation. We denote the RLVR fine-tuned model by π_{ft} and the corresponding base model by π_{ref} . To prepare for the inference, for each query q , we sample N responses from each model, i.e., $\{o_i^{ft}\}_{i=1}^N \sim \pi_{ft}(\cdot | q)$ and $\{o_i^{ref}\}_{i=1}^N \sim \pi_{ref}(\cdot | q)$, respectively. These samples enable us to analyze behavioral changes induced by RLVR fine-tuning.

According to the gradient coefficient $m_{i,t}$ in Equation (5), we quantify behavioral divergence along two axes: advantage side and divergence side. These correspond to the two main components in policy updates in RLVR, i.e., reward-driven selection and probability adjustment.

Feature - Advantage Signal. Let \mathcal{R} be the rule-based evaluator, e.g., mathematical verification. We examine how the model’s ability to generate correct outputs evolves from the base model to the fine-tuned model. Specifically, for a given prompt q , we measure the change in expected reward across sampled responses, which reflects shifts in the advantage signal induced by RLVR fine-tuning.

$$s_q^{Adv} = \underbrace{\frac{1}{N} \sum_{i=1}^N \mathcal{R}(o_i^{ft})}_{\text{FT Score}} - \underbrace{\frac{1}{N} \sum_{i=1}^N \mathcal{R}(o_i^{ref})}_{\text{Base Score}}$$

Feature - Divergence Signal. As the second component, we analyze the logit-side divergence, which reflects changes in token-level probabilities beyond what is explained by reward improvement alone. Together, these capture subtle but systematic changes in generation behavior that contribute to membership leakage.

- **K3 Divergence.** We then consider a fundamental signal: the divergence between π_{ft} and π_{ref} for the generated answer, which captures how the policy shifts during fine-tuning. To estimate the KL divergence reliably and with reduced variance, we adopt k3 [35], an unbiased estimator of KL divergence. For a single response o_i^{ft} sampled from the fine-tuned model π_{ft} , the token-level k3 divergence is computed as:

$$s_{q,o_i^{ft}}^{KL} = \frac{1}{|o_i|} \sum_{t=1}^{|o_i|} \frac{\pi_{ref}(o_{i,t} | q, o_{<t})}{\pi_{ft}(o_{i,t} | q, o_{<t})} - \log \frac{\pi_{ref}(o_{i,t} | q, o_{<t})}{\pi_{ft}(o_{i,t} | q, o_{<t})} - 1.$$

The prompt-level divergence is then obtained by averaging over all sampled responses $\{o_j^{ft}\}_{j=1}^N \sim \pi_{ft}(\cdot | q)$. This feature is referred to as `Divergence` in the following text.

- **Likelihood.** Besides the direct estimation of divergence, we additionally select the calibrated likelihood as an empirical indicator of behavioral change. While traditional likelihood overfitting is less pronounced in RLVR due to the absence of golden answers, the fine-tuned model may still assign systematically higher (or lower) probabilities to certain outputs depending on reward feedback. Similar to LiRA [29], we compute the likelihood ratio between π_{ft} and π_{ref} on sampled responses:

$$s_q^{LiRA} = \frac{1}{N} \sum_{i=1}^N [\log \pi_{ft}(o_i^{ft} | q) - \log \pi_{ref}(o_i^{ft} | q)],$$

where $\{o_j^{ft}\}_{j=1}^N \sim \pi_{ft}(\cdot | q)$. The calibrated feature is referred to as `Likelihood` in the following text.

This metric captures whether the policy becomes more confident in its outputs post-finetuning, which is a subtle but measurable signature of training exposure. We further enhance robustness to surface-level redundancy by incorporating zlib normalization [25]. The zlib-normalized likelihood difference is defined as:

$$s_q^{Zlib} = \frac{1}{N} \sum_{i=1}^N \frac{\log \pi_{ft}(o_i^{ft} | q) - \log \pi_{ref}(o_i^{ft} | q)}{|\text{zlib.compress}(o_i)|},$$

where the denominator reflects the compressed length of the response. The calibrated feature is referred to as `Zlib` in the following text.

- **Prediction.** We train a stacking classifier to perform membership inference using the concatenated feature vectors. The base estimators—random forest and logistic regression with

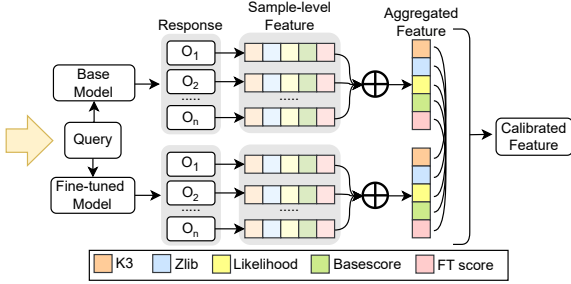


Figure 2: Overview of DIBA’s feature construction.

standardization—are trained on the input features, and their predictions are combined via a meta-learner (logistic regression) using cross-validated stacking to minimize overfitting. The final model is fit on the entire training set of selected features and used to predict membership probabilities for test samples, leveraging complementary signals from both models.

6 Attack Evaluation

Models. Regarding RLVR, we select two widely used models: Qwen-2.5-7B-Instruct and Qwen-2.5-3B-Instruct [12], both of which have been extensively adopted in recent studies on verifiable reasoning and reward-guided training [9,36,37]. The Qwen series is chosen due to its strong performance on mathematical tasks, as well as its widespread use in the RL community, making it an ideal testbed for privacy analysis in modern LLM fine-tuning paradigms.

Datasets. Regarding the dataset, we use different parts of MATH dataset [32] and its variant [33], the most widely adopted benchmark in RLVR research, which comprises competition-level math problems, to construct our membership inference evaluation. Specifically, to prevent potential data leakage from training-time exposure, we draw both member and non-member prompts exclusively from the test split of the original dataset, ensuring that these examples were not seen during pre-training or fine-tuning.

Training Setups. To conduct the RL training, we utilize verl [38] as the training framework, which greatly accelerates the rollout and training stages. Specifically, we consider 2 widely used RLVR algorithms, i.e., GRPO [1] and DAPO [9]. Regarding the training hyperparameters, we use the recommended parameters in verl library and show the details in Section D. The model is trained on 4 NVIDIA H100 GPUs, with each full 60-epoch run taking approximately 18 hours to complete.

Evaluation Metrics. We report multiple metrics to comprehensively assess membership inference performance following previous work [16,29]: balanced accuracy, AUC, log-scaled ROC curves, and TPR@0.1%FPR. All quantitative results are obtained via 5-fold cross-validation. For each fold, the predictor is trained and evaluated on stratified splits of member and non-member prompts. Numerical metrics (AUC, balanced accuracy, TPR@FPR) are reported as the mean across five independent runs, all conducted with a fixed

Table 2: Accuracy (ACC) and TPR@0.1%FPR for DIBA on different models and training algorithms.

Model	Metric	GRPO		DAPO	
		ACC	TPR@0.1%FPR	ACC	TPR@0.1%FPR
Qwen-2.5-3b	FT Score	0.640	0.002	0.744	0.003
	Base Score	0.552	0.002	0.552	0.002
	Divergence	0.461	0.000	0.488	0.000
	Zlib	0.560	0.000	0.541	0.000
	Likelihood	0.549	0.008	0.500	0.008
	DIBA		0.659	0.073	0.762
Qwen-2.5-7b	FT Score	0.659	0.002	0.721	0.002
	Base Score	0.553	0.001	0.553	0.001
	Divergence	0.455	0.003	0.524	0.003
	Zlib	0.530	0.000	0.549	0.000
	Likelihood	0.537	0.003	0.518	0.000
	DIBA		0.673	0.084	0.740

random seed for reproducibility. The *implementation details* are shown in Section D.

6.1 Main Evaluation

Figure 3 presents the attack performance of DIBA and its component features, several of which correspond to enhanced baseline signals inspired by LoRA-Leak [17]. The TPR@0.1% FPR is reported in Table 2. Overall, DIBA significantly all individual baselines and feature-based variants in both AUC and TPR@0.1%FPR, demonstrating the effectiveness of our integrated approach. Across different RLVR algorithms, models fine-tuned with DAPO exhibit higher vulnerability to membership inference compared to those trained with GRPO. This increased exposure may stem from DAPO’s more effective training dynamics and stronger learning capacity, leading to larger behavioral shifts from the base model, a phenomenon we analyze further in Section 6.2. When comparing model sizes, we observe no consistent trend in whether larger models leak more membership information. This suggests that scale alone does not linearly correlate with privacy risk in the RLVR setting.

Additionally, we observe that the TPR@0.1%FPR achieved by DIBA is significantly higher by an order of magnitude at least than that obtained by any individual feature alone. This substantial gain suggests a synergistic interaction among features, where complementary signals enhance detection power in the high-precision regime. We further analyze the contribution and interplay of these features in Section 6.3.

6.2 Effect of Model Fitting

We examine how the AUC evolves during training to understand the emergence of membership signals. We define train reward as the accuracy on responses sampled from member prompts, i.e., those used in RLVR fine-tuning, reflecting the model’s performance on seen data. In contrast, test reward measures accuracy on non-member prompts, capturing generalization to unseen inputs.

As shown in Figure 4, at the beginning of training, train and test rewards are nearly identical, indicating minimal behavioral difference between member and non-member prompts. Consequently, membership inference performance (AUC) remains close to random. As training progresses,

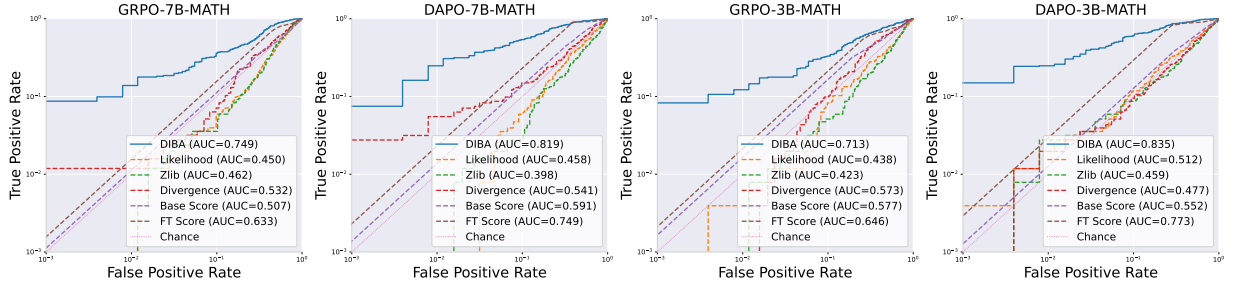


Figure 3: AUC and log-scale ROC curves for DIBA on different models and training algorithms.

however, the two trajectories diverge: the model rapidly improves on member prompts due to repeated exposure and reward feedback, while performance on non-members improves more slowly, driven only by generalization. This growing reward gap correlates with rising AUC, showing that membership distinguishability increases with training step. Intuitively, the more a prompt benefits from policy optimization, the more detectable its membership becomes.

Overfitting or Learning. Crucially, this increase in AUC does not stem from classical overfitting, such as memorizing specific outputs, as seen in supervised settings. Instead, it arises from the progressive learning dynamics inherent to RLVR. The RLVR training framework inherently resists output-level overfitting. Because gradients are driven by advantage rather than direct likelihood maximization, there is no mechanism that systematically reinforces a single fixed response for a given prompt across epochs. Once the generated responses for a prompt have all correct answers, the gradient will become very small or close to 0 (because the advantage becomes zero and the regularization coefficient β is very small). This stands in sharp contrast to SFT, where each training step explicitly boosts the likelihood of the ground-truth answer, leading to memorization signals.

Specifically, we attribute the rising AUC to the exploratory nature of RLVR. In early stages, the model often fails to generate correct solutions, even for member prompts, so the behavioral divergence does not emerge at all. As training proceeds, successful responses are reinforced through policy updates, gradually increasing the probability of correct outputs. This learned improvement is both prompt-specific and behaviorally persistent, creating a detectable signal: member prompts are those for which the model has successfully internalized effective solution paths.

6.3 Analysis on Feature Importance

To understand the factors driving membership leakage in RLVR, we conduct a progressive analysis of DIBA’s feature components, examining their roles across different detection regimes, i.e., from overall ranking to high-precision identification and hard-case behavior.

Overall Discriminative Power. We begin by analyzing DIBA’s performance in terms of AUC, which captures the attack’s overall ability to rank member prompts above non-members without strict false positive constraints. As shown in Figure 3, among all feature components, the FT Score, which measures the improvement in rule-based correctness

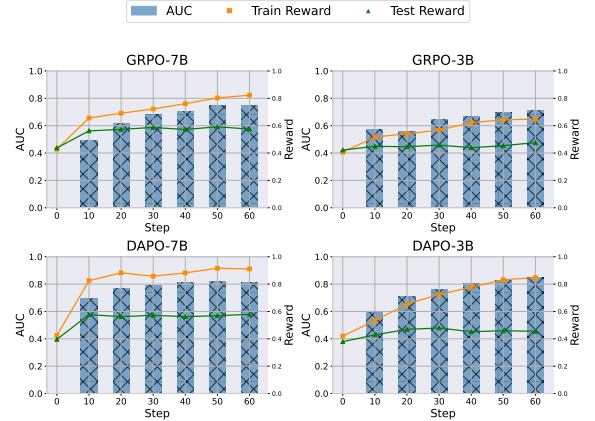


Figure 4: Performance Over Steps: Train reward represents the accuracy on sampled responses from the member prompts, while test reward represents the sampled responses from the non-member prompts.

from base to fine-tuned model, achieves significantly higher AUC than other signals. This reflects the central role of reward-driven behavioral change in membership leakage: prompts that induce consistent performance gains during RLVR training are globally more distinguishable.

However, high AUC alone does not imply practical utility under privacy-sensitive conditions. For instance, at FPR of 0.1%, it achieves almost zero TPR in the GRPO-7B-MATH setting, while DIBA achieves a TPR of 0.084, over an order of magnitude higher. This mismatch reveals a critical limitation: while FT Score effectively separates populations on average, it lacks the calibration needed to identify the most elusive members under strict thresholds.

Low-FPR Performance. In privacy-sensitive scenarios, attackers must operate at extremely low false positive rates. To evaluate this regime, we adopt a Pareto analysis (Figure 5) using pAUC (0–0.1% FPR) and TPR@threshold, with point size reflecting tail separation (KStail). Here, Divergence, which quantifies the KL shift from base to fine-tuned policy, emerges as the most effective single feature, consistently achieving the highest TPR and occupying the Pareto frontier across model variants. Likelihood and Zlib provide meaningful but secondary contributions. In contrast, FT Score yields zero TPR despite high pAUC, indicating it ranks positives well but fails to generate extreme outlier scores necessary for thresholding. This makes it ineffective in isola-

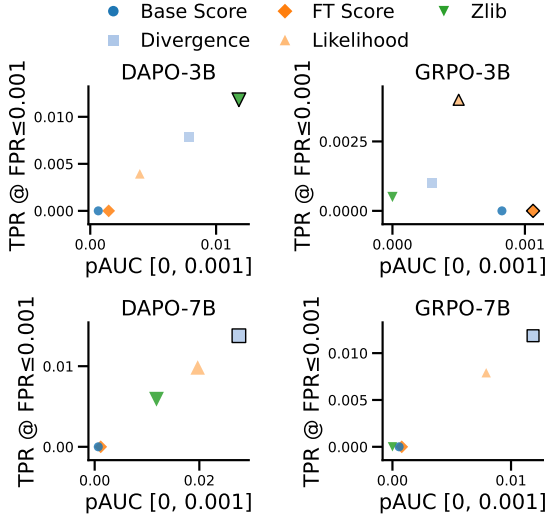


Figure 5: Pareto Front Visualization of Feature Performance: pAUC and TPR@FPR $\leq 0.1\%$ are on the axes. Marker size reflects the KS statistic (larger = higher), and black rings indicate Pareto-optimal features.

tion—but highly valuable when combined. These results establish a key principle: low-FPR detection relies more on calibrated signals.

Ideal Behavior of TPs. To understand how DIBA succeeds on clear true positives (TPs), those correctly identified at an extremely low FPR of 0.1%, we examine how each feature of these TPs compares to the negative class distribution. For each TP, we compute the percentile rank of its feature value within the negative distribution (see Figure 6).

On the advantage side, clear TPs show a significant increase from Base Score to FT Score, indicating that fine-tuning meaningfully improved correctness on these prompts. This large improvement serves as a strong signal of training exposure. On the logit side, these instances consistently display high divergence and likelihood values, typically ranking above the 80th percentile of the non-member (negative) distribution. This indicates substantial token-level shifts in policy behavior, providing calibrated, high-confidence evidence for membership. The only exception is the DAPO-3B model, where TP feature values fall into low percentiles relative to negatives. Despite the counterintuitive direction, the separation in percentile space is extreme and highly consistent, enabling confident detection. These patterns can be further exploited for future work to guide data augmentation or feature engineering. Additionally, we conduct an ablation study on removing one feature at a time, and the results are shown in Section E.

6.4 Analysis on Example Hardness

To understand example hardness in membership inference for RLVR, we analyze the from two perspectives, i.e., analytically hard and false-positive driven hard examples.

Analytically Hard Examples. We revisit the gradient coefficient of GRPO (Equation (5)), which consists of two com-

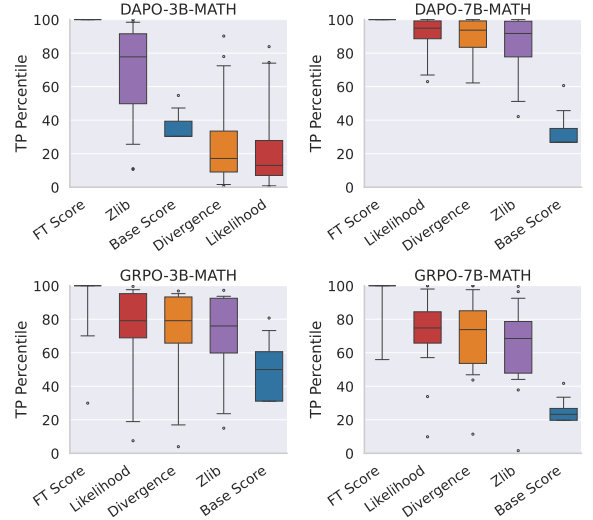


Figure 6: TP Percentile: Distribution of feature percentile ranks (vs. negatives) for true positives detected at 0.1% FPR, across four runs.

ponents: the advantage term and the KL divergence regularization term. Given that the regularization coefficient β is typically small (e.g., $1e-3$), the advantage term dominates the policy update. The group-normalized advantage $\hat{A}_{i,t} = \frac{r_i - \text{mean}(\mathbf{r})}{\text{std}(\mathbf{r})}$ becomes zero when all responses in a batch receive the same rewards, i.e., when all are correct (all-1) or all are incorrect (all-0). In such cases, the gradient signal diminishes, resulting in minimal parameter updates beyond KL regularization toward the reference model. Consequently, prompts that consistently yield high or low rewards across training contribute little to policy adaptation and are thus expected to be harder to identify as members.

To validate this hypothesis, we partition the evaluation set into three subsets based on behavioral consistency:

- **All-1:** Prompts where the base and fine-tuned models both achieve an average score of 1 (consistently correct).
- **All-0:** Prompts where both models achieve an average score of 0 (consistently incorrect).
- **Residual:** All other prompts exhibiting performance changes during training.

For each subset, we train a dedicated membership predictor using DIBA. Results in Table 3 confirm our hypothesis:

Table 3: Membership Inference Performance in Each Subset: The performance in AUC and TPR@0.1%FPR is the average of stratified folds.

Model	Split	GRPO			DAPO		
		# Samples	AUC	TPR @ 0.1% FPR	# Samples	AUC	TPR@0.1%FPR
Math-3b	All-0	108	0.687	0.047	95	0.559	0.000
	All-1	119	0.551	0.028	118	0.518	0.014
	Residual	281	0.765	0.130	294	0.912	0.282
	Unified	508	0.713	0.073	508	0.834	0.154
Math-7b	All-0	76	0.661	0.064	69	0.528	0.030
	All-1	191	0.525	0.005	189	0.485	0.016
	Residual	240	0.877	0.162	250	0.937	0.280
	Unified	508	0.750	0.084	508	0.819	0.107

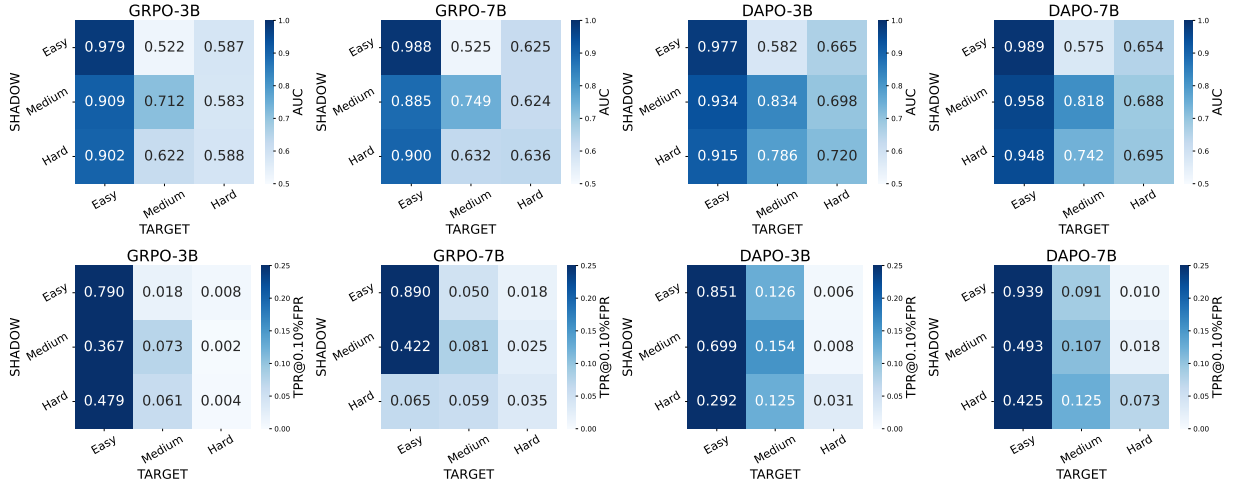


Figure 7: AUC (upper) And TPR@0.1%FPR (lower) performance of transferring across different datasets

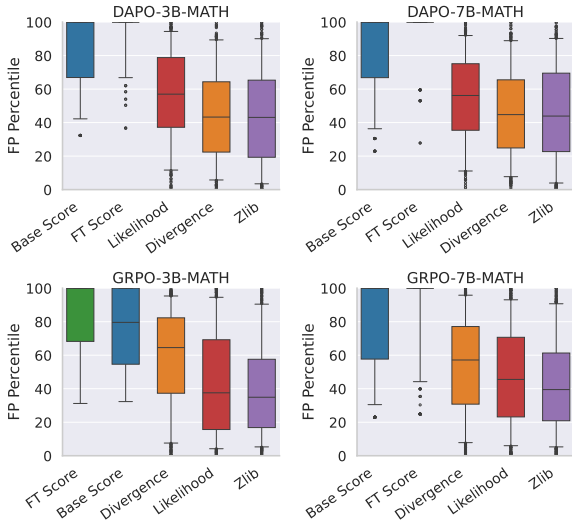


Figure 8: False Positive Percentiles: Distribution of feature percentile ranks for all false positives.

the All-1 and All-0 subsets exhibit significantly lower AUC and TPR@0.1%FPR compared to the Residual group, indicating reduced membership signal. Notably, the All-1 subset proves even harder than All-0, counterintuitive at first glance, since one might expect failed predictions to leak less information. We attribute this asymmetry to response similarity before and after fine-tuning. Using Rouge-L and 3-gram overlap as similarity metrics (Figure 17), we find that in the All-1 subset, responses from the fine-tuned model are substantially more similar to those from the base model, showing a 50% higher Rouge-L score and 20% higher n-gram overlap compared to other groups. This high stability indicates minimal behavioral shift despite correct generation, leading to weaker leakage signals.

False-Positive Example Analysis. We further examine the characteristics of false positive (FP) predictions by analyzing the percentile ranks of each feature for FP examples relative to the full set of non-member instances. As shown in Figure 8, the error pattern is consistent across models and set-

tings. On the advantage side, FPs typically exhibit very high FT Score (close to 1) and relatively high Base Score (often near or above 0.8). This indicates that the model was already highly likely to solve these prompts correctly before fine-tuning, and RLVR training further solidified this behavior. Since DIBA relies on improvement in correctness as a key signal, such cases are misclassified because the behavioral shift mimics that of true members, even though the prompt was not in the training set. At the same time, on the logit side, these examples show only moderate to low divergence and likelihood scores, typically below the 50th percentile. As a result, the logit-side features fail to provide sufficient evidence to override the strong advantage signal.

Together, this creates a challenging failure mode: DIBA mistakes generalization on inherently easy, high-skill prompts for training exposure. These results highlight a fundamental limitation, that when fine-tuning amplifies pre-existing capabilities rather than introducing new ones, behavioral divergence becomes ambiguous.

6.5 Shadow Training

In this section, we study a scenario where the adversary knows the training algorithm and model architecture but has no access to data from the same distribution as the target dataset. This is a realistic assumption in many practical settings, such as when public models are fine-tuned on proprietary or confidential data.

Shadow Data. Due to the high computational cost of RLVR training, it is impractical to train multiple shadow models for transferability analysis. Given the fitting level analysis in Section 6.2, we construct two datasets, i.e., hard and easy, with deliberately different levels of generalization hardness. Crucially, the terms “hard” and “easy” refer not to the inherent difficulty of the questions; instead, it is used to describe the extent to which improvement in member data can generalize to nonmember data. Detailed definitions of the two subsets are shown in Section F. The data used in the previous evaluation is referred to as “medium” data, which shows moderate generalization from member data to nonmember

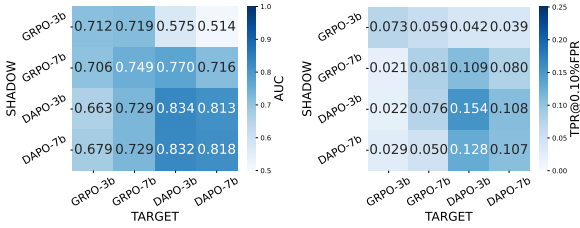


Figure 9: Cross model/algorithm transferability of DIBA.

data. In-distribution evaluation and reward analysis results (provided in Section F) confirm the stated difficulty in the membership inference scenario.

Evaluation. The transferability results are shown in Figure 7 (AUC and TPR@0.1%FPR). We find that for a given target dataset, training the DIBA predictor on a shadow dataset of matched hardness yields significantly better performance than using a shadow dataset of mismatched difficulty. For instance, despite the nearly perfect in-distribution AUC on the easy dataset (approaching 1.0), transferring this detector to the harder dataset leads to a sharp drop in performance, where the AUC degrades to approximately 0.6, with even greater deterioration in high-precision regimes (TPR@0.1%FPR). In contrast, detectors trained on the hard dataset maintain strong performance when applied to the easy dataset, achieving competitive AUC and higher robustness in low-FPR settings.

These findings highlight that the effectiveness of MIA in RLVR is not only dependent on model behavior but also critically shaped by the representational consistency of the training data.

6.6 Model/Algorithm Transferring

In this section, we study a scenario where the adversary aims to determine whether a specific dataset was used to train a model, despite having no knowledge of the model’s training algorithm or architecture. This is a realistic assumption in many practical settings, such as when auditing publicly released models with opaque training histories.

Specifically, we investigate cross-model and cross-algorithm transferability of the DIBA detector, assessing its generalization across different model sizes (3B vs. 7B) and training algorithms (GRPO vs. DAPO). The results, visualized as heatmaps in Figure 9, reveal several key patterns. First, the in-distribution setting, where the detector is trained and evaluated on models with matching size and algorithm, achieves the highest performance in most cases. Second, model size has a relatively small impact within the same algorithm: detectors transfer reasonably well between 3B and 7B variants under DAPO or GRPO alone, suggesting that scaling does not drastically alter the nature of leakage.

In contrast, cross-algorithm transfer exhibits significantly sharper degradation, particularly in TPR@0.1%FPR. A detector trained on GRPO struggles to identify members in DAPO-finetuned models, and vice versa. This suggests that different RLVR algorithms shape the policy in fundamentally distinct ways. Notably, models trained with DAPO (both 3B

and 7B) consistently act as better source models: detectors trained on DAPO generalize more effectively to other models. This indicates that DAPO induces more consistent, stable, and potentially stronger membership signals across architectures.

6.7 Ablation Study

In this section, we conduct an ablation study to understand how the specific settings in DIBA may affect the final membership inference performance.

Generated Samples. Since DIBA relies on sampling multiple responses to compute both advantage and logit-level features, we conduct an ablation study on the number of generated responses per prompt (k). Ablation results in Figure 10 are averaged over five independent runs, with shaded regions indicating the full range from minimum to maximum performance. When k is small, attack performance is suboptimal, as few samples inadequately capture the model’s true behavioral distribution and problem-solving ability. We observe that AUC saturates quickly, showing diminishing returns beyond $k=4$, while TPR@1%FPR continues to improve with larger k , indicating that higher sample counts enhance the precision of outlier detection in the low-FPR regime by better characterizing tail behaviors. As a result, we set $k=8$ for all experiments in this paper.

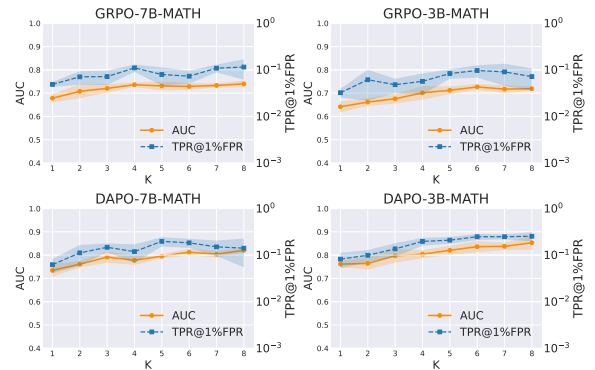


Figure 10: Ablation study on sampled responses.

Sampling Temperatures. Another key hyperparameter in DIBA is the sampling temperature. Since feature estimation relies on representative response distributions, the choice of temperature directly impacts the fidelity of behavioral change measurement. Results in Figure 11 show the AUC and TPR@0.1%FPR across different temperatures. We observe that temperature has only a modest effect on AUC: performance tends to be slightly lower at low temperatures.

In contrast, TPR@0.1%FPR is highly sensitive to temperature, with performance varying by up to a factor of two across settings. This suggests that tail behavior is critical for high-precision detection. At very high temperatures, excessive noise may obscure consistent policy shifts, while at very low temperatures, lack of variation limits the ability to detect subtle but systematic changes. Balancing robustness in both overall discrimination and high-precision detection, we find that a moderate temperature range (0.5–0.7) achieves optimal trade-offs. In this paper, we use $T = 0.5$ to ensure sufficient

diversity while maintaining coherent and verifiable outputs.

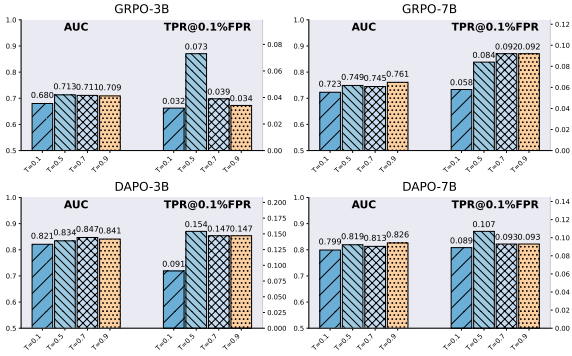


Figure 11: Ablation study on sampling temperatures.

Response Source. When calculating the logit side features, we base the calculation on responses sampled from the fine-tuned model. To assess the impact of this choice, we evaluate an alternative variant in which responses are instead sampled from the base model. Results, shown in Table 4, indicate that using fine-tuned model responses consistently yields higher TPR@0.1%FPR across settings. Therefore, in this work, we adopt responses from the fine-tuned model to compute all logit-side divergence features.

Table 4: Ablation study on response sources.

Model	Response	GRPO		DAPO	
		AUC	TPR@0.1%FPR	AUC	TPR@0.1%FPR
Math-3b	Base	0.704	0.036	0.846	0.113
	Fine-tuned	0.712	0.073	0.834	0.154
Math-7b	Base	0.764	0.076	0.809	0.113
	Fine-tuned	0.749	0.084	0.818	0.107

6.8 Adaptation to VLMs

In this section, we explore the feasibility of adapting DIBA to vision-language models (VLMs), extending our membership inference framework beyond text-only settings.

Models. We use Qwen-2.5-7B-VL-Instruct [2], a state-of-the-art vision-language model, as the base architecture for fine-tuning. This model supports joint reasoning over textual prompts and visual inputs, making it suitable for geometry problem-solving tasks under the RLVR paradigm.

Dataset. We evaluate on the Geo-3k dataset [39], which contains high-school-level geometry problems accompanied by graphical illustrations. Each instance requires multimodal understanding and deductive reasoning. To ensure clean evaluation and prevent data leakage, all prompts—both member and non-member—are drawn from the test split of Geo-3k, following the same protocol as in the language-only setting. The *training setup* and *implementation details* are shown in Section G.

Main Evaluation. The attack performance of DIBA on vision-language models (VLMs) is shown in Figure 12 and Table 11 (in Appendix). We observe that DIBA achieves a competitive performance of approximately 0.7 AUC, which

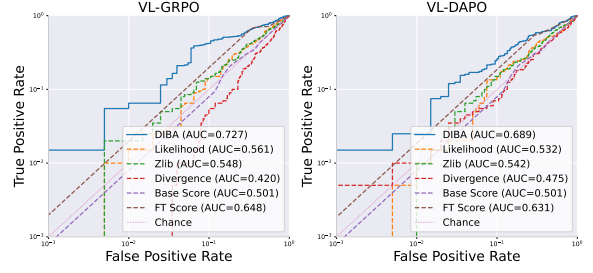


Figure 12: AUC and Log-scale ROC curves on VLMs.

is similar to the performance observed on language-only LLMs, indicating that the core membership signals remain detectable in multimodal settings. However, two key differences emerge.

First, performance in privacy-sensitive, low-FPR regimes is notably weaker, with TPR@0.1%FPR dropping from the 1e-1 range (as seen in LLMs) to the 1e-2 range. This suggests that while the FT Score continues to provide moderate discriminative power, the logit-level divergence metrics, which are designed for text modality, fail to fully capture the subtle behavioral shifts in VLMs, particularly in the tail distribution. The added complexity of visual encoding and cross-modal alignment may obscure these signals, limiting high-precision detection. We leave the VLM-specific MIA design to future work.

Second, we observe that DAPO does not exhibit increased privacy leakage on VLMs, as it does on LLMs, likely due to incomplete implementation support (e.g., lack of overlong buffer handling) and consequently suboptimal training dynamics. Since membership inference fundamentally depends on strong model fitting to training data, the reduced exposure is not a limitation of DIBA, but rather a reflection of poorer training efficiency under current RLVR frameworks for VLMs. In other words, the model fails to learn robustly from its training set, thereby reducing the strength of any membership signal.

Fitting Level. We also examine the training dynamics and fitting behavior of RLVR in VLMs. Compared to language-only LLMs, VLMs require significantly longer training epochs to achieve a good fit, often around 100 epochs under GRPO. This slower convergence reflects the added complexity of aligning visual inputs with reasoning trajectories. Notably, in DAPO, we observe negative average train rewards. This stems from the design of its reward function, which assigns explicit negative feedback to incorrect outputs rather than neutral (zero) rewards as in GRPO.

Crucially, we find that membership inference performance remains strongly correlated with the reward gap (0.7 AUC on the training set and 0.46 on the test set), the difference between train and test reward. Larger gaps correspond to higher attack performance, consistent with our findings on LLMs. This confirms that, even in the multimodal setting, membership leakage in RLVR is driven by how much the model learns from its training data.

The analysis on example hardness and ablation study on VLMs are shown in Section G, and the conclusion drawn on

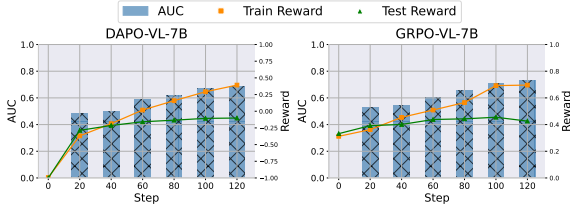


Figure 13: Performance over steps.

LLMs typically applies to VLMs as well.

7 Defense

To mitigate the membership leakage in RLVR, we investigate several defenses against DIBA.

Training Regularization. Since DIBA exploits the behavioral divergence between the base and fine-tuned models, an intuitive defense is to strengthen regularization during training. According to Table 5, we find that stronger regularization has only a marginal effect on membership inference performance in most cases. AUC and TPR@0.1%FPR remain largely unchanged across models and algorithms, indicating that moderate KL penalties do not effectively suppress leakage. The sole exception is the Qwen-3B model trained with GRPO, which exhibits a notable drop in TPR@0.1%FPR under high β . Upon further analysis, we observe that, in this case, the train reward degrades closely to the base model level (0.422), suggesting that the model fails to learn meaningful improvements on the training data. This lack of learning—rather than effective regularization—leads to minimal behavioral change, making membership signals nearly undetectable. In other words, the observed privacy gain stems not from robustness, but from underfitting: when the model does not meaningfully adapt to its training data, there is little to leak. As a result, for well-trained models, simply increasing β is insufficient to prevent membership inference, underscoring the resilience of DIBA to such defensive tuning.

Response Perturbation. We explore response perturbation to obscure the consistency of generated outputs. Specifically, we consider two perturbations, i.e., character transformations and paraphrase attacks. Regarding the character transformations, we employ a set of character perturbations, such as character swaps and deletions, and the results are shown in Table 12 (in Appendix). A fixed perturbation budget is applied per response, with individual operation specified in

Table 5: Defense Evaluation Against Perturbation: AUC and TPR@0.1%FPR of DIBA against regularization. DAPO sets $\beta = 0$ for default. Reward represents the accuracy on the test set.

Model	β	Math-3b (Reward 0.422)			Math-7b (Reward 0.430)		
		AUC	TPR@0.1% FPR	Reward	AUC	TPR@0.1% FPR	Reward
GRPO	0.1	0.649	0.006	0.526	0.729	0.122	0.705
	0.01	0.672	0.003	0.593	0.728	0.121	0.774
	0.001	0.712	0.073	0.648	0.749	0.084	0.823
DAPO	0.1	0.835	0.151	0.812	OOM		
	0.01	0.828	0.128	0.832			
	0.0	0.834	0.154	0.846	0.818	0.107	0.911

Table 6: Performance Against Paraphrase Attack

Model	Attack	GRPO		DAPO	
		AUC	TPR@0.1% FPR	AUC	TPR@0.1% FPR
Math-3b	Original	0.712	0.073	0.834	0.154
	Paraphrased	0.545	0.003	0.668	0.012
Math-7b	Original	0.749	0.084	0.818	0.107
	Paraphrased	0.587	0.012	0.658	0.020

Section H. Under varying perturbation strengths, DIBA is robust and maintains most performance with a moderate perturbation strength of 0.02 to 0.05. When the strength increases to 0.1, i.e., 10% characters are changed, performance degrades largely, but this kind of perturbation also increases perplexity by a factor of $3\times$. Regarding the paraphrase attack, we rewrite the response with Llama3-3B-Instruct [7], and the results are shown Table 6. For both models and algorithms, a paraphrase attack can greatly reduce the privacy leakage by 20% in AUC and more in TPR@0.1%FPR, while keeping the original accuracy. However, the paraphrase attack would introduce significantly longer generation cost, thus limiting the realistic application.

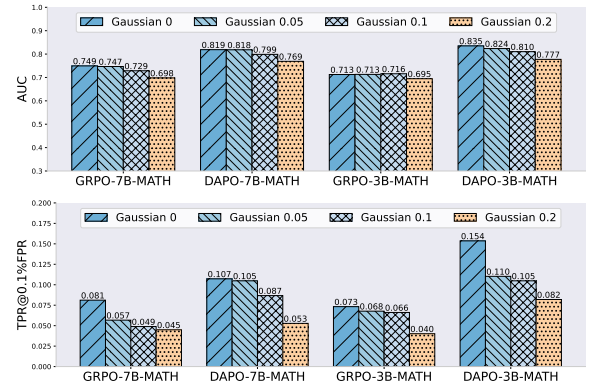


Figure 14: AUC and TPR@0.1%FPR of DIBA against local DP with different Gaussian noise.

Local Differential Privacy. Given the absence of established differential privacy (DP) methods for RLVR and the infeasibility of directly adapting gradient-based approaches to verl framework, we explore two lightweight local DP methods that inject randomness before token decoding [40] and DIBA classifier training [41], respectively. We establish theoretical bounds under Laplace and Gaussian noises (see Section H) and evaluate the empirical performance.

Table 7: Performance in differentially private decoding.

Model	Strength	GRPO		DAPO	
		AUC	TPR@0.1%FPR	AUC	TPR@0.1%FPR
Math-3b	0	0.712	0.073	0.834	0.154
	0.01	0.715	0.034	0.837	0.111
	0.05	0.714	0.040	0.837	0.171
	0.1	0.709	0.056	0.844	0.109
Math-7b	0	0.749	0.084	0.818	0.107
	0.01	0.758	0.082	0.803	0.100
	0.05	0.759	0.048	0.822	0.073
	0.1	0.747	0.071	0.822	0.112

The first setting simulates the differentially private decoding (Table 7). Surprisingly, we find that private decoding shows no effect even when the noise is big (0.1), except the moderate degradation of $\text{TPR}@0.1\% \text{FPR}$ in some cases. This might be because the RLVR process reduces the entropy [36], so that tokens with high probability can always be selected even when being perturbed. The second setting simulates a scenario where the verifier is noisy or infeasible, and the model vendors may provide perturbed logits to keep the utility. Figure 14 shows that even 20% perturbation causes only a modest degradation in AUC (around 5%) and halfly reduction in $\text{TPR}@0.1\% \text{FPR}$. The results of the Laplacian noise setting are in Figure 20 (in Appendix). This indicates that DIBA is also relatively robust against the local DP setting.

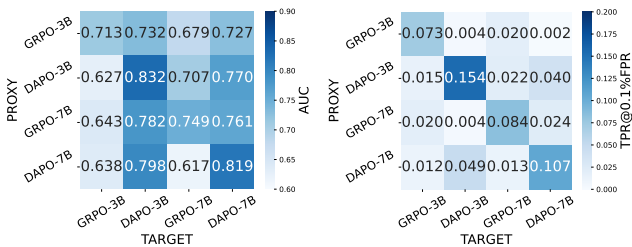


Figure 15: Black-box performance of DIBA.

8 Discussions and Limitations

Black-box Setting. We investigate the feasibility of applying DIBA in a black-box setting, where the adversary only has access to generated text from the base and fine-tuned models, without knowledge of model architecture, size, or training algorithm. In this scenario, logit-side features cannot be computed directly and must instead be estimated using a proxy model. Without loss of generality, we consider each model as a proxy model and evaluate the transferring performance to different models, and the results are shown in Figure 15. We find that when the proxy is trained with DAPO, DIBA achieves non-trivial membership inference performance, significantly above random guessing. In contrast, GRPO-trained proxies yield very weak signals, with $\text{TPR}@0.1\% \text{FPR}$ often below 0.01. This suggests that DAPO induces more generalizable behavioral patterns, which are better captured even by mismatched proxies. Nevertheless, a significant performance gap remains between black-box and grey-box settings. For future work, it will be crucial to develop more robust methods for estimating behavioral change under complete uncertainty about model size and training dynamics.

Datasets, Algorithm, and Models. We use math-related datasets as our primary benchmark due to their widespread adoption in RLVR research. To evaluate the transferability in DIBA, we extend DIBA to an instruction-following dataset [42], where rewards are computed based on whether generated responses adhere to given instructions (see Section I). Results shown in Figure 16 demonstrate that DIBA achieves competitive performance on both 3B and 7B mod-

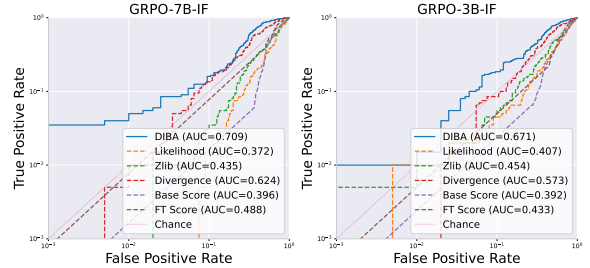


Figure 16: Adaptation to instruction-following dataset.

els, with AUC around 0.7 and non-trivial $\text{TPR}@0.1\% \text{FPR}$ exceeding 0.01. These findings suggest that behavioral divergence, as captured by DIBA, is not limited to mathematical reasoning but extends to other RLVR applications. We encourage future work to explore its applicability across a broader range of domains, including safety alignment, planning, and multimodal instruction following. For algorithms, we focus on GRPO and DAPO, two of the most commonly used and representative RLVR methods in recent work. Our models are drawn from the Qwen series (e.g., Qwen-3B and Qwen-7B), which are widely adopted in both research and practice for verifiable reasoning tasks.

While our study provides a systematic analysis within this well-established setting, we acknowledge that broader generalization requires future exploration across additional datasets, architectures, and training algorithms.

9 Conclusion

In this paper, we uncover a unique privacy risk inherent in RLVR, addressing a challenging threat model where only prompts, not responses, are targeted. To tackle this setting, we propose a novel membership inference attack, DIBA. As RLVR becomes central to aligning advanced AI systems, DIBA enables auditing of benchmark leakage and data contamination in published models.

Ethics Considerations

This work highlights critical privacy risks in RLVR, a paradigm increasingly used to arm large language models with advanced reasoning capabilities. While RLVR avoids explicit supervision and reference answers, our attack DIBA demonstrates that behavioral changes induced by training can still leak information. This raises ethical concerns regarding data confidentiality, especially when training data contains sensitive, personal, or proprietary content.

We emphasize that this research is intended to improve understanding of privacy vulnerabilities and strengthen defenses, not to enable harmful exploitation. The release of any implementation will follow responsible disclosure practices, limited to academic use with appropriate safeguards. We hope this work encourages the community to develop more privacy-preserving RLVR methods and to consider behavioral leakage as a legitimate risk in future alignment efforts.

References

- [1] Z. Shao, P. Wang, Q. Zhu, R. Xu, J. Song, X. Bi, H. Zhang, M. Zhang, Y. Li, Y. Wu *et al.*, “Deepseekmath: Pushing the limits of mathematical reasoning in open language models,” *arXiv preprint arXiv:2402.03300*, 2024. 1, 2, 3, 6
- [2] S. Bai, K. Chen, X. Liu, J. Wang, W. Ge, S. Song, K. Dang, P. Wang, S. Wang, J. Tang *et al.*, “Qwen2. 5-v1 technical report,” *arXiv preprint arXiv:2502.13923*, 2025. 1, 11
- [3] Y. Liu, Z. Zhong, Y. Liao, Z. Sun, J. Zheng, J. Wei, Q. Gong, F. Tong, Y. Chen, Y. Zhang *et al.*, “On the generalization and adaptation ability of machine-generated text detectors in academic writing,” in *Proceedings of the 31st ACM SIGKDD Conference on Knowledge Discovery and Data Mining V. 2*, 2025, pp. 5674–5685. 1, 2
- [4] B. Hui, J. Yang, Z. Cui, J. Yang, D. Liu, L. Zhang, T. Liu, J. Zhang, B. Yu, K. Lu *et al.*, “Qwen2. 5-coder technical report,” *arXiv preprint arXiv:2409.12186*, 2024. 1, 2
- [5] J. Achiam, S. Adler, S. Agarwal, L. Ahmad, I. Akkaya, F. L. Aleman, D. Almeida, J. Altenschmidt, S. Altman, S. Anadkat *et al.*, “Gpt-4 technical report,” *arXiv preprint arXiv:2303.08774*, 2023. 1, 2
- [6] L. Ouyang, J. Wu, X. Jiang, D. Almeida, C. Wainwright, P. Mishkin, C. Zhang, S. Agarwal, K. Slama, A. Ray *et al.*, “Training language models to follow instructions with human feedback,” *Advances in neural information processing systems*, vol. 35, pp. 27 730–27 744, 2022. 1, 2
- [7] A. Dubey, A. Jauhri, A. Pandey, A. Kadian, A. Al-Dahle, A. Letman, A. Mathur, A. Schelten, A. Yang, A. Fan *et al.*, “The llama 3 herd of models,” *arXiv e-prints*, pp. arXiv–2407, 2024. 1, 12
- [8] X. Wen, Z. Liu, S. Zheng, Z. Xu, S. Ye, Z. Wu, X. Liang, Y. Wang, J. Li, Z. Miao *et al.*, “Reinforcement learning with verifiable rewards implicitly incentivizes correct reasoning in base llms,” *arXiv preprint arXiv:2506.14245*, 2025. 1
- [9] Q. Yu, Z. Zhang, R. Zhu, Y. Yuan, X. Zuo, Y. Yue, W. Dai, T. Fan, G. Liu, L. Liu *et al.*, “Dapo: An open-source llm reinforcement learning system at scale,” *arXiv preprint arXiv:2503.14476*, 2025. 1, 2, 3, 6
- [10] S. S. Srivastava and V. Aggarwal, “A technical survey of reinforcement learning techniques for large language models,” *CoRR*, vol. abs/2507.04136, 2025. 1
- [11] K. Team, Y. Bai, Y. Bao, G. Chen, J. Chen, N. Chen, R. Chen, Y. Chen, Y. Chen, Y. Chen *et al.*, “Kimi k2: Open agentic intelligence,” *arXiv preprint arXiv:2507.20534*, 2025. 1, 2
- [12] A. Yang, B. Yang, B. Hui, B. Zheng, B. Yu, C. Zhou, C. Li, C. Li, D. Liu, F. Huang *et al.*, “Qwen2 technical report, 2024,” URL <https://arxiv.org/abs/2407.10671>, vol. 7, p. 8, 2024. 1, 6
- [13] R. Xie, J. Wang, R. Huang, M. Zhang, R. Ge, J. Pei, N. Z. Gong, and B. Dhingra, “Recall: Membership inference via relative conditional log-likelihoods,” *arXiv preprint arXiv:2406.15968*, 2024. 1, 2, 4
- [14] J. Zhang, J. Sun, E. Yeats, Y. Ouyang, M. Kuo, J. Zhang, H. F. Yang, and H. Li, “Min-k%+ : Improved baseline for detecting pre-training data from large language models,” *arXiv preprint arXiv:2404.02936*, 2024. 1, 2, 4
- [15] Q. Feng, S. R. Kasa, S. K. Kasa, H. Yun, C. H. Teo, and S. B. Bodapati, “Exposing privacy gaps: Membership inference attack on preference data for llm alignment,” *arXiv preprint arXiv:2407.06443*, 2024. 1, 3, 4
- [16] W. Fu, H. Wang, C. Gao, G. Liu, Y. Li, and T. Jiang, “Practical membership inference attacks against fine-tuned large language models via self-prompt calibration,” *arXiv preprint arXiv:2311.06062*, 2023. 1, 3, 4, 6
- [17] D. Ran, X. He, T. Cong, A. Wang, Q. Li, and X. Wang, “Lora-leak: Membership inference attacks against lora fine-tuned language models,” *arXiv preprint arXiv:2507.18302*, 2025. 1, 3, 4, 6, 16
- [18] T. Chu, Y. Zhai, J. Yang, S. Tong, S. Xie, D. Schuurmans, Q. V. Le, S. Levine, and Y. Ma, “Sft memorizes, rl generalizes: A comparative study of foundation model post-training,” *arXiv preprint arXiv:2501.17161*, 2025. 2
- [19] Y. Bai, A. Jones, K. Ndousse, A. Askell, A. Chen, N. DasSarma, D. Drain, S. Fort, D. Ganguli, T. Henighan *et al.*, “Training a helpful and harmless assistant with reinforcement learning from human feedback,” *arXiv preprint arXiv:2204.05862*, 2022. 2, 16
- [20] R. Rafailov, A. Sharma, E. Mitchell, C. D. Manning, S. Ermon, and C. Finn, “Direct preference optimization: Your language model is secretly a reward model,” *Advances in neural information processing systems*, vol. 36, pp. 53 728–53 741, 2023. 2, 16
- [21] J. Schulman, F. Wolski, P. Dhariwal, A. Radford, and O. Klimov, “Proximal policy optimization algorithms,” *arXiv preprint arXiv:1707.06347*, 2017. 2, 16
- [22] Y. Liu, J. Zheng, Z. Sun, Z. Peng, W. Dong, Z. Sha, S. Cui, W. Wang, and X. He, “Thought manipulation: External thought can be efficient for large reasoning models,” *arXiv preprint arXiv:2504.13626*, 2025. 2
- [23] W. Shi, A. Ajith, M. Xia, Y. Huang, D. Liu, T. Blevins, D. Chen, and L. Zettlemoyer, “Detecting pretraining data from large language models,” *arXiv preprint arXiv:2310.16789*, 2023. 2
- [24] J. Mattern, F. Miresghallah, Z. Jin, B. Schölkopf, M. Sachan, and T. Berg-Kirkpatrick, “Membership inference attacks against language models via neighbour-

- hood comparison,” *arXiv preprint arXiv:2305.18462*, 2023. 2, 4
- [25] N. Carlini, F. Tramer, E. Wallace, M. Jagielski, A. Herbert-Voss, K. Lee, A. Roberts, T. Brown, D. Song, U. Erlingsson *et al.*, “Extracting training data from large language models,” in *30th USENIX security symposium (USENIX Security 21)*, 2021, pp. 2633–2650. 2, 5, 16
- [26] A. Radford, J. Wu, R. Child, D. Luan, D. Amodei, I. Sutskever *et al.*, “Language models are unsupervised multitask learners,” *OpenAI blog*, vol. 1, no. 8, p. 9, 2019. 3
- [27] S. Biderman, H. Schoelkopf, Q. G. Anthony, H. Bradley, K. O’Brien, E. Hallahan, M. A. Khan, S. Purohit, U. S. Prashanth, E. Raff *et al.*, “Pythia: A suite for analyzing large language models across training and scaling,” in *International Conference on Machine Learning*. PMLR, 2023, pp. 2397–2430. 3
- [28] Y. Dong, X. Jiang, H. Liu, Z. Jin, B. Gu, M. Yang, and G. Li, “Generalization or memorization: Data contamination and trustworthy evaluation for large language models,” *arXiv preprint arXiv:2402.15938*, 2024. 3, 4
- [29] N. Carlini, S. Chien, M. Nasr, S. Song, A. Terzis, and F. Tramer, “Membership inference attacks from first principles,” in *2022 IEEE symposium on security and privacy (SP)*. IEEE, 2022, pp. 1897–1914. 4, 5, 6, 16
- [30] Meta, “Llama-license,” 2025. [Online]. Available: <https://github.com/meta-llama/llama-models/blob/main/models/llama4/LICENSE> 4
- [31] Alibaba, “Qwen-license,” 2025. [Online]. Available: <https://hf-mirror.com/Qwen/Qwen2.5-Math-7B/blob/main/LICENSE> 4
- [32] D. Hendrycks, C. Burns, S. Kadavath, A. Arora, S. Basart, E. Tang, D. Song, and J. Steinhardt, “Measuring mathematical problem solving with the math dataset,” *arXiv preprint arXiv:2103.03874*, 2021. 4, 6
- [33] J. LI, E. Beeching, L. Tunstall, B. Lipkin, R. Soletskyi, S. C. Huang, K. Rasul, L. Yu, A. Jiang, Z. Shen, Z. Qin, B. Dong, L. Zhou, Y. Fleureau, G. Lample, and S. Polu, “Numinamath,” [<https://huggingface.co/AI-MO/NuminaMath-1.5>](https://github.com/project-numina/aimo-progress-prize/blob/main/report/numina_dataset.pdf), 2024. 4, 6, 17
- [34] C. White, S. Dooley, M. Roberts, A. Pal, B. Feuer, S. Jain, R. Shwartz-Ziv, N. Jain, K. Saifullah, S. Dey, Shubh-Agrawal, S. S. Sandha, S. V. Naidu, C. Hegde, Y. LeCun, T. Goldstein, W. Neiswanger, and M. Goldblum, “Livebench: A challenging, contamination-free LLM benchmark,” in *The Thirteenth International Conference on Learning Representations*, 2025. 4
- [35] J. Schulman, “Approximating kl divergence,” 2020. [Online]. Available: <http://joschu.net/blog/kl-approx.html> 5
- [36] G. Cui, Y. Zhang, J. Chen, L. Yuan, Z. Wang, Y. Zuo, H. Li, Y. Fan, H. Chen, W. Chen *et al.*, “The entropy mechanism of reinforcement learning for reasoning language models,” *arXiv preprint arXiv:2505.22617*, 2025. 6, 13
- [37] R. Shao, S. S. Li, R. Xin, S. Geng, Y. Wang, S. Oh, S. S. Du, N. Lambert, S. Min, R. Krishna *et al.*, “Spurious rewards: Rethinking training signals in rlvr,” *arXiv preprint arXiv:2506.10947*, 2025. 6
- [38] G. Sheng, C. Zhang, Z. Ye, X. Wu, W. Zhang, R. Zhang, Y. Peng, H. Lin, and C. Wu, “Hybridflow: A flexible and efficient rlhf framework,” *arXiv preprint arXiv:2409.19256*, 2024. 6
- [39] P. Lu, R. Gong, S. Jiang, L. Qiu, S. Huang, X. Liang, and S.-C. Zhu, “Inter-gps: Interpretable geometry problem solving with formal language and symbolic reasoning,” in *The Joint Conference of the 59th Annual Meeting of the Association for Computational Linguistics and the 11th International Joint Conference on Natural Language Processing (ACL-IJCNLP 2021)*, 2021. 11
- [40] J. Majumdar, C. Dupuy, C. Peris, S. Smaili, R. Gupta, and R. Zemel, “Differentially private decoding in large language models,” *arXiv preprint arXiv:2205.13621*, 2022. 12
- [41] Y. Xue, R. Zhong, J. Li, Y. Chen, and Y. Liu, “Privacy-preserving mobile edge generation: Analog and digital transmission,” *IEEE Transactions on Vehicular Technology*, pp. 1–6, 2025. 12
- [42] J. Ye, C. Huang, Z. Chen, W. Fu, C. Yang, L. Yang, Y. Wu, P. Wang, M. Zhou, X. Yang *et al.*, “A multi-dimensional constraint framework for evaluating and improving instruction following in large language models,” *arXiv preprint arXiv:2505.07591*, 2025. 13, 20
- [43] S. Yeom, I. Giacomelli, M. Fredrikson, and S. Jha, “Privacy risk in machine learning: Analyzing the connection to overfitting,” in *2018 IEEE 31st computer security foundations symposium (CSF)*. IEEE, 2018, pp. 268–282. 16
- [44] Y. Liu, M. Ott, N. Goyal, J. Du, M. Joshi, D. Chen, O. Levy, M. Lewis, L. Zettlemoyer, and V. Stoyanov, “Roberta: A robustly optimized bert pretraining approach,” 2019. [Online]. Available: <https://arxiv.org/abs/1907.11692> 16
- [45] C. Dwork, “Differential privacy,” in *International colloquium on automata, languages, and programming*. Springer, 2006, pp. 1–12. 19, 20
- [46] K. Wei, J. Li, M. Ding, C. Ma, H. H. Yang, F. Farokhi, S. Jin, T. Q. Quek, and H. V. Poor, “Federated learning with differential privacy: Algorithms and performance analysis,” *IEEE transactions on information forensics and security*, vol. 15, pp. 3454–3469, 2020. 19
- [47] J. Zhou, T. Lu, S. Mishra, S. Brahma, S. Basu, Y. Luan, D. Zhou, and L. Hou, “Instruction-following

evaluation for large language models,” *arXiv preprint arXiv:2311.07911*, 2023. 20

A Related work

- **LOSS [43]:** The simplest baseline uses the negative log-likelihood (NLL) under the target model:

$$\text{Score}_{\text{LOSS}}(q) = -\log \pi_{\theta}(q) = -\sum_{i=1}^{|q|} \log \pi_{\theta}(q_i | q_{<i}).$$

A threshold τ is chosen (e.g., via validation data), and q is classified as a member if $\text{Score}_{\text{LOSS}}(q) \leq \tau$.

- **LiRA [29]:** Compares the target model’s likelihood to that of a reference model $\pi_{\theta_{\text{ref}}}$ trained on disjoint data:

$$\text{Score}_{\text{LiRA}}(q) = \log \pi_{\theta}(q) - \log \pi_{\theta_{\text{ref}}}(q),$$

where higher scores indicate membership.

- **Zlib [25]:** Normalizes the model loss by the text’s compressibility using the zlib algorithm. Let $\text{zlib}(q)$ be the compressed size (in bits) of q . Then:

$$\text{Score}_{\text{zlib}}(q) = \frac{-\log \pi_{\theta}(q)}{\text{zlib}(q)},$$

where lower values suggest membership.

- **Min-k%:** Uses only the $k\%$ of tokens with the lowest per-token loss. Let $\mathcal{T}_k(q)$ be the set of indices of these tokens. Then:

$$\text{Score}_{\text{Min-}k\%}(q) = -\frac{1}{|\mathcal{T}_k(q)|} \sum_{i \in \mathcal{T}_k(q)} \log \pi_{\theta}(q_i | q_{<i}),$$

where higher scores (i.e., lower average loss on predictable tokens) indicate membership.

B Preliminary for RL

PPO [21]. It is one of the most widely used on-policy reinforcement learning algorithms in the context of LLM alignment [19]. To stabilize training, PPO assumes that the model only has a single update following each exploration stage. Specifically, for a prompt q and generated response $o = (o_1, \dots, o_T)$, PPO computes an advantage A_t for each token o_t , which measures how much better or worse the token is compared to the average behavior under the current policy. The advantage is typically estimated using a separate value network, which predicts the expected future reward. The PPO objective is:

$$\mathcal{J}(\theta) = \mathbb{E}_{[q, o \sim \pi_{\theta, \text{old}}]} \sum_{t=1}^{|o|} \frac{\pi_{\theta}(o_t | q, o_{<t})}{\pi_{\theta, \text{old}}(o_t | q, o_{<t})} A_t, \quad (6)$$

A key drawback of PPO is that the training may involve an additional value network of comparable size, which doubles memory usage and complicates training.

DPO [20]. It offers a simpler alternative to PPO by eliminating the need for an explicit reward model or value model.

Instead, DPO directly optimizes the policy using human or model-generated preference data, where each prompt is paired with a chosen and rejected response. Specifically, it encourages the model to assign higher probabilities to preferred responses and lower probabilities to dispreferred ones, without updating any reward or value function. The DPO objective is:

$$\mathcal{J}(\theta) = \mathbb{E}_{[q, o^{\pm}]} \log \sigma \left(\beta \frac{1}{|o^+|} \sum_{t=1}^{|o^+|} \log \frac{\pi_{\theta}(o_t^+ | q, o_{<t}^+)}{\pi_{\text{ref}}(o_t^+ | q, o_{<t}^+)} - \beta \frac{1}{|o^-|} \sum_{t=1}^{|o^-|} \log \frac{\pi_{\theta}(o_t^- | q, o_{<t}^-)}{\pi_{\text{ref}}(o_t^- | q, o_{<t}^-)} \right), \quad (7)$$

where o^+ and o^- are the chosen and rejected outputs in the dataset, π_{ref} is a reference model (e.g., the initial model), β controls the strength of regularization, and σ is the sigmoid function. Given the computational efficiency and stability, DPO is a popular choice for offline preference tuning.

C Baseline Implementation

For the neighbor baseline, we use RoBERTa-base [44] to encode each prompt and retrieve the 8 nearest neighbors based on cosine similarity in the embedding space. For the min-k% baseline, we set $k=0.2$. To calibrate each method, we compute the relevant metric (e.g., likelihood, entropy) separately on responses generated by the base and fine-tuned models, then take the difference: $\text{metric}_{\text{ft}} - \text{metric}_{\text{ref}}$. As shown in prior work [17], this calibration effectively removes biases present in the pre-trained model and isolates changes due to fine-tuning. Such calibration can improve performance in low-FPR regimes.

D Hyperparameters

RLVR Setup. Both GRPO and DAPO use a training batch size of 512 prompts and generate 16 responses per prompt. They share the same learning rate (1e-6), max prompt length (GRPO: 1024; DAPO: 2048), and max response length (GRPO: 2048; DAPO: 8192). Both employ PPO mode in verl with a mini-batch size of 512 (GRPO) or 32 (DAPO). The micro batch size on each GPU is set to 8 for both algorithms to avoid out-of-memory errors. KL loss and reward KL are turned off in DAPO; while GRPO uses KL loss with a coefficient of 0.001. DAPO introduces asymmetric PPO clipping (clip ratios [0.2, 0.28]) and uses token-mean loss aggregation, while GRPO uses standard symmetric clipping. Both run for 60 epochs on 4 GPUs per node with vLLM-based rollout and gradient checkpointing enabled.

Implementation Details. During response generation, we sample 8 distinct responses per prompt using temperature 0.5, top-p sampling with $p = 0.9$, and a repetition penalty of 1.05 to balance diversity and coherence. For each response, we compute sample-level features, which are then aggregated at the prompt level.

For the predictor, we utilize a stacking classifier that combines a Random Forest (with 100 trees) and a Logistic Regression pipeline (which includes median imputation with

missing indicators and column-wise standard scaling) as base estimators to generate meta-features. The final estimator is a Logistic Regression model trained on these meta-features to produce the final prediction.

E Feature Importance

To understand the effect of each feature component, we conduct an ablation study by removing one feature at a time. We find that sequentially removing the logit-side feature degrades the TPR@0.1%FPR performance. When only the Ft Score is left, the metrics drops to zero.

Table 8: Ablation study on removing component features of DIBA.

Ablation Setting	TPR@0.1%FPR
Baseline (all features)	15.4%
- Remove zlib	15.3%
- Remove Divergence	14.6%
- Remove Likelihood	11.4%
- Remove Base Score	0.0%

E.1 Hard Example

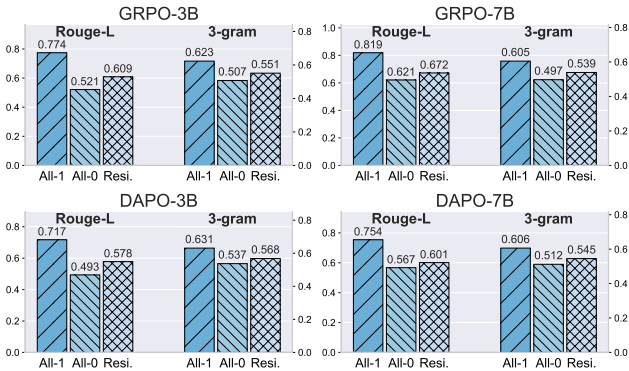


Figure 17: Similarity Between Responses Generated by Fine-tuned Model and Base Model: For each prompt, we generate 8 responses, and compute the group Rouge-L and 3-gram to get the prompt-level similarity, then average over the whole dataset (both member and non-member data).

F Shadow Training

Dataset. For the hard dataset, we use a synthetic variant of MATH [33] in which prompts and solutions are systematically paraphrased to increase linguistic and structural complexity, making generalization more challenging. For the easy dataset, we sample directly from the original MATH training set, preserving its natural formulation and higher learnability. From both sets, we select 1,000 members and 1,000 non-member prompts. The dataset in the main evaluation is treated as the medium dataset.

In-distribution Performance. The in-distribution performance of DIBA on the two shadow datasets is shown in Figure 18. We observe a significant performance gap between them: the easy dataset achieves near-perfect AUC and TPR@0.1%FPR, while the hard dataset exhibits substantially lower detection performance. To understand this discrepancy, we analyze the results from the perspective of training dynamics and generalization. As shown in Table 9, the difference in detectability correlates with the degree of generalization exhibited by the model during RLVR training. On the easy dataset, the model generalizes poorly, leading to higher performance improvement on member prompts than non-member ones. In contrast, the hard dataset generalizes well, resulting in a smaller reward gap. This reduces the reward gap between train and test sets, weakening the behavioral divergence signal and making membership harder to detect. Thus, membership distinguishability is not solely determined by training exposure, but by the extent to which learning fails to generalize.

G Adaptation to VLMs

Training Setups. We apply GRPO and DAPO for fine-tuning the VLM using rule-based rewards (e.g., answer correctness via symbolic verification). However, due to limited optimization of current RL frameworks (e.g., verl) for VLMs, training is significantly slower (40 hours for GRPO and 68 hours for DAPO) and less stable compared to language-only models. Notably, a key component, the overlong response buffer, in DAPO is not yet supported for VLMs, limiting the full replication of advanced training dynamics. Despite these challenges, we successfully complete RLVR training and observe measurable policy improvement on the task.

Implementation Details. We sample 8 responses per prompt using temperature 0.5, top-p=0.9, and a repetition penalty of 1.05. All input images are resized to 448x448 and encoded using the built-in vision tower. The predictor is trained using the same stacking classifier as the previous setting.

Analysis on Example Hardness. We extend the example hardness analysis from Section 6.4 to the VLM setting, with results presented in Table 10. The significant performance gap across splits confirms the validity of our hardness characterization: prompts that are consistently incorrect (All-0) or consistently correct (All-1) across training, i.e., those inducing minimal policy updates, remain challenging for membership inference. Both groups exhibit AUC scores close to 0.5, indicating near random-guess performance. This aligns with findings in the language-only setting and underscores that, even in multimodal RLVR, examples with little behavioral shift contribute weak leakage signals, making them inherently harder to distinguish as members. The results reinforce that membership distinguishability in VLMs, as in LLMs, is driven by measurable changes in model behavior rather than static input properties.

Ablation on Temperature and Samples. The ablation studies on sampling temperature and the number of generated responses for VLMs are presented in Figure 19. Regarding sampling temperature, we find that T=0.7 achieves

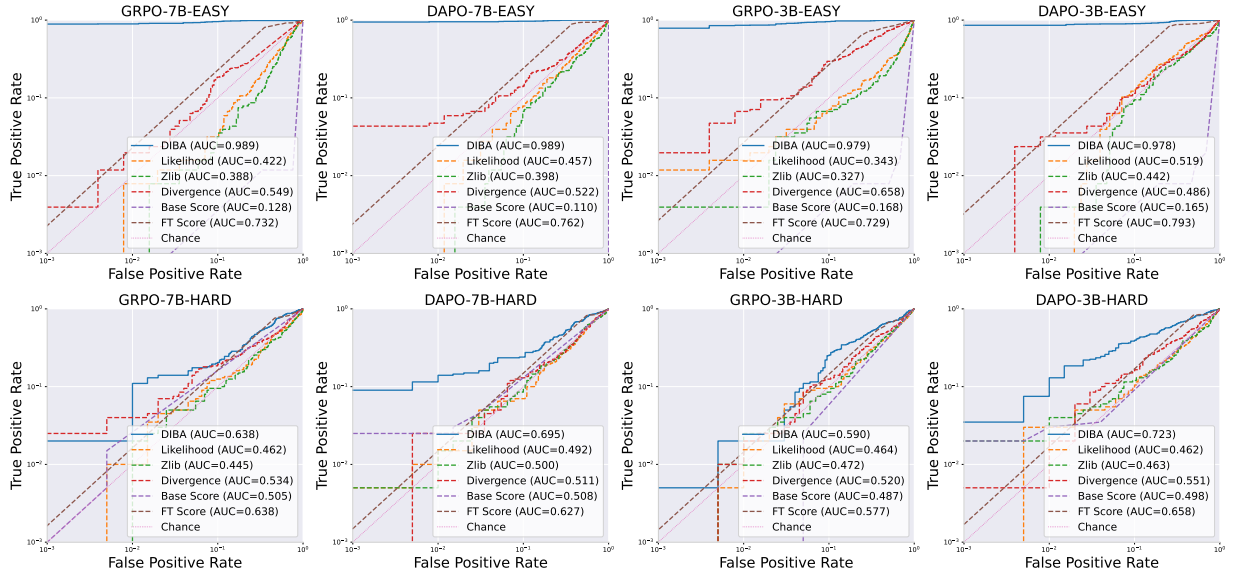


Figure 18: In-distribution results of shadow datasets

Table 9: Train and test reward before and after training.

Model	Easy				Hard			
	Begin		End		Begin		End	
	Train Reward	Test Reward						
GRPO-3B	0.521	0.406	0.779	0.459	0.490	0.486	0.671	0.565
DAPO-3B	0.541	0.379	0.882	0.449	0.495	0.486	0.839	0.558
GRPO-7B	0.469	0.437	0.893	0.565	0.482	0.487	0.754	0.621
DAPO-7B	0.493	0.396	0.938	0.563	0.481	0.467	0.848	0.612

Table 10: Hard Example Analysis on VLMs.

Model	Split	GRPO			DAPO		
		# Samples	AUC	TPR@0.1%FPR	# Samples	AUC	TPR@0.1%FPR
VL-7b	All-0	111	0.527	0.046	115	0.492	0.032
	All-1	47	0.477	0.042	47	0.382	0.067
	Residual	243	0.807	0.078	239	0.771	0.059
	Unified	400	0.728	0.050	400	0.691	0.034

Table 11: Accuracy (ACC) and TPR@0.1%FPR for DIBA on VLMs.

Model	Metric	GRPO		DAPO	
		ACC	TPR@0.1%FPR	ACC	TPR@0.1%FPR
VL-7b	FT Score	0.663	0.002	0.646	0.002
	Base Score	0.474	0.002	0.474	0.001
	Divergence	0.514	0.002	0.498	0.010
	Entropy	0.477	0.013	0.513	0.003
	Likelihood	0.516	0.013	0.508	0.003
	DIBA	0.679	0.050	0.643	0.034

the best overall trade-off, yielding high AUC and stable TPR@0.1%FPR. While the DAPO model at T=0.1 exhibits an anomalously high TPR in one run, we treat this as noise: at such a low temperature, generation becomes nearly deterministic (akin to greedy decoding), with minimal response diversity. This limits reliable estimation of behavioral divergence and advantage signals, making the outlier result likely coincidental rather than indicative of improved detection.

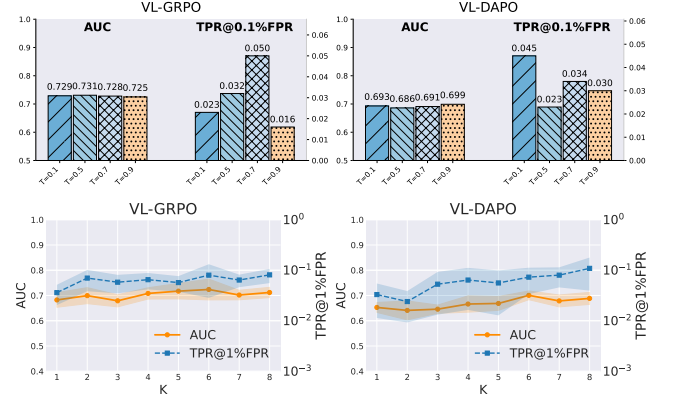
For the number of sampled responses, the trend mirrors our findings in the LLM setting: increasing k provides diminishing returns in AUC, but continues to improve TPR@0.1%FPR significantly. This confirms that more samples better capture the tail behavior of the policy, enhancing precision in high-threshold regimes. Based on this analysis, we retain k=8 as the default number of responses for VLM evaluation, ensuring robust feature estimation without excessive computational cost.

H Defense

Perturbation Config. We stochastically apply the following operations with the indicated probabilities within the perturbation budget.

- Character swap (p=20%): Randomly swap two adjacent characters (e.g., “hello” → “hlelo”).
- Character deletion (p=10%): Randomly remove a character from the text (e.g., “text” → “tet”).
- Keyboard-style typos (p=10%): Replace a character with one of its neighboring keys on a QWERTY keyboard (e.g., “cat” → “cay”).
- Random casing (p=30%): Randomly toggle the case of individual letters (e.g., “Hello” → “hELlo”).
- Punctuation insertion (p=10%): Insert a random punctuation mark at a random position (e.g., “hi” → “hi!”), modeling accidental keystrokes.
- Punctuation removal (p=10%): Delete existing punctuation marks (e.g., “What?” → “What”).

- Double whitespace injection (p=10%): Insert an extra space between words or tokens.


Figure 19: Ablation study on sampling temperature.

Response Perturbation.

Table 12: Defense Evaluation Against Perturbation: AUC and TPR@0.1% FPR of DIBA against response perturbation of different strength.

Model	Strength	GRPO			DAPO		
		AUC	TPR@0.1% FPR	PPL	AUC	TPR@0.1% FPR	PPL
Math-3b	0	0.712	0.073	1.09	0.834	0.154	1.15
	0.02	0.696	0.041	1.63	0.825	0.115	1.81
	0.05	0.662	0.027	2.26	0.789	0.093	2.53
	0.1	0.635	0.013	3.35	0.768	0.076	3.80
Math-7b	0	0.749	0.084	1.13	0.818	0.107	1.19
	0.02	0.729	0.019	1.66	0.782	0.078	1.75
	0.05	0.710	0.017	2.27	0.756	0.067	2.41
	0.1	0.679	0.008	3.33	0.728	0.055	3.55

Local Differential Privacy. We first establish the theoretical bound for the local DP setting.

Definition 1. ((ϵ, δ)-DP [45]) A randomized mechanism \mathcal{A} satisfies (ϵ, δ)-differential privacy if for any two neighboring inputs \mathbf{f} and \mathbf{f}' that differ in at most one element, and for any measurable output set S ,

$$\Pr[\mathcal{A}(\mathbf{f}) \in S] \leq e^\epsilon \cdot \Pr[\mathcal{A}(\mathbf{f}') \in S] + \delta, \quad (8)$$

where $\epsilon > 0$ denotes the privacy budget, and δ is a relaxation parameter [45].

In practice, we adopt the Gaussian mechanism, defined as $\mathcal{A}(\mathbf{f}) = \mathbf{f} + \mathcal{N}(0, \sigma^2 \mathbf{I})$, which guarantees (ϵ, δ)-DP, when the noise standard deviation σ satisfies the condition derived in [46]:

$$\sigma \geq \frac{\sqrt{2 \ln(1.25/\delta)} \cdot \Delta}{\epsilon}, \quad (9)$$

where $\Delta = \max_{\mathbf{f}, \mathbf{f}'} \|\mathbf{f} - \mathbf{f}'\|_2$ is the ℓ_2 -sensitivity of the feature mapping. Assume $\|\mathbf{f}\|_2 \leq C$, we can get the ℓ_2 -sensitivity can be bounded as $\Delta \leq 2C$. Therefore,

$$\epsilon \geq \frac{2C \sqrt{2 \ln(1.25/\delta)}}{\sigma}. \quad (10)$$

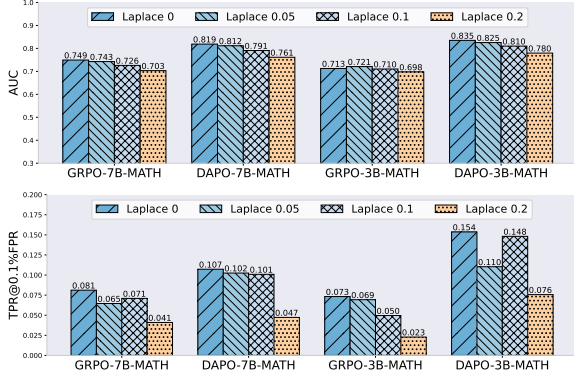


Figure 20: AUC and TPR@0.1%FPR of DIBA against local DP with different Laplacian noises.

For the Laplace mechanism, it is defined as $\mathcal{A}(\mathbf{f}) = \mathbf{f} + \text{Lap}(\mathbf{0}, b)$, which guarantees ϵ -differential privacy, where $\text{Lap}(\mathbf{0}, b)$ denotes independent Laplace noise with scale b added to each feature dimension [45]. The noise scale b is determined according to the ℓ_1 -sensitivity of the feature mapping: $b \geq \frac{\Delta_1}{\epsilon}$, where $\Delta_1 = \max_{\mathbf{f}, \mathbf{f}'} \|\mathbf{f} - \mathbf{f}'\|_1$ is the ℓ_1 -sensitivity of the feature vector. Assuming that each feature vector satisfies $\|\mathbf{f}\|_1 \leq C_1$, the ℓ_1 -sensitivity can be bounded as $\Delta_1 \leq 2C_1$. Therefore, the achievable privacy budget satisfies $\epsilon \geq \frac{2C_1}{b}$. We report the defense performance of adding Laplacian noise to the extracted feature in Figure 20.

I Instruction Following Dataset

MulDimIF [42] performs constraint expansion, conflict detection, and instruction rewriting based on the IFEval dataset [47], yielding a set of code-verifiable instruction-following test samples. The training setting is the same as previous GRPO training, with epoch set to 2 and batch size set to 32.